19th International Conference on
Adaptive Structures and Technologies
October 6-9, 2008
Ascona, Switzerland

Damage sensing in a self-healing material using fibre Bragg grating sensors

Kirkby E., de Oliveira R., Michaud V., Månson J.A. *
Laboratoire de Technologie des Composites et Polymères, Institut des Matériaux, Ecole Polytechnique Fédérale de Lausanne, CH-1015, Lausanne, Suisse
*Tel: +41 21 693 42 81, fax: +41 21 693 58 80, email: jan-anders.manson@epfl.ch

ABSTRACT

We report on the localisation of an impact event on a carbon fibre composite plate using three surface-mounted fibre Bragg grating (FBG) sensors to monitor ultrasonic Lamb waves. We combine a novel wavelength-intensity conversion technique that allows fast-sampling of the FBGs, and an algorithm for localising an impact on an orthotropic plate. We are capable of locating the impact to a precision of a few millimetres. To our knowledge, this is the first time this combination has been developed, which could find applications for combined health monitoring and impact localisation.

Keywords: Fibre Bragg grating, remote sensing, impact localisation, fast-sampling, Lamb wave.

1. INTRODUCTION

Carbon fibre composite materials have a high specific strength and stiffness in the direction of the reinforcing fibres, making them attractive to the aerospace, automotive, marine and sports industries, for example. However, due to their anisotropy, they have relatively poor properties in the transverse direction, with notably low resistance to impact. Impact events are inevitable during the lifetime of a composite structure, occurring during both service and maintenance, in the form of collisions with stones or birds, for example. Such events can cause extensive internal delaminations, where two adjacent lamina become de-bonded. This damage, while often difficult or even impossible to detect at the surface of the material, severely degrades the load-bearing capacity of the structure.

To address this issue, the development of self-healing polymers and composites has begun over the last ten years. For example, White *et al.* store a liquid healing agent (dicyclopentadiene - DCPD) in microcapsules and a solid catalyst (Grubbs' first generation catalyst) in wax beads, both embedded in the matrix [1]. Upon damage, the crack propagates, rupturing the microcapsules in its path. This allows the healing agent to spread over the crack face, where it polymerises on contact with the catalyst, repairing the crack. It has recently been shown that the healed properties of the matrix are improved by embedding shape memory alloy (SMA) wires and activating them during the healing period, as they both close the crack and heat the healing agent during polymerisation [2]. To know when to activate the wires and to limit their activation to the affected area, however, the location of the damage needs to be known.

This can be achieved by monitoring the elastic ultrasonic waves that are generated in thin plates as a

result of an impact event, known as Lamb waves [3]. There are two main categories of Lamb waves, which propagate with two different modes: (i) extensional mode, causing out-of-plane deformations that are symmetric about the mid-plane of the plate and (ii) flexural mode, causing out-of-plane deformations that are anti-symmetric about the mid-plane of the plate. The propagation of these waves is dependent on the mechanical properties and the density of the plate material, e. g. [4]. Furthermore, they are dispersive, meaning that their velocity depends on their frequency. Both are infinite in number, although when the product of the wave frequency and the sample thickness is below 1 MHz mm, only the fundamental modes (known as S_0 and A_0) can propagate [5].

Lamb waves can be detected with either surface-mounted or embedded sensors. To date, piezo-ceramic transducers (PZT) have been the sensors of choice, as they have high sensitivity to ultrasonic waves. However, fibre optic sensors, and specifically fibre Bragg grating (FBG) sensors, represent today an attractive alternative for structural health monitoring. The key advantages are that optical fibres are robust, lightweight, small and easily placed between composite plies [6, 7], they require no electrical power at the sensing point and are immune to electromagnetic interference, eliminating the need for costly and heavy shielding. Furthermore, a single optical fibre can be multiplexed to monitor dozens of points along its length [8, 9].

FBGs have successfully been used to detect transverse cracks and delaminations in carbon-fibre reinforced polymers, by interrogating them at a rate of a few hertz [10]-[12]. However, to be used in this new application as remote impact event sensors, the FBG output signal needs to be fast-sampled. The velocity of this strain pulse is typically 1,000-7,000 m/s in a polymer composite. The timing of the leading edge of the strain pulse therefore needs to be measured to about 1 μs, implying a sampling rate of at least 1 MHz. As a consequence, novel ultrasonic readout systems for FBG sensors are being developed to make these sensors suitable for structural health monitoring applications, e. g. [13]–[20].

The first steps toward acousto-ultrasonic sensing with fibre Bragg grating sensors were made by Betz *et al.* [13]–[15]. In their initial work, they glued both PZT transducers and FBG sensors on the surface of a PMMA plate. The FBG sensors were interrogated using a narrow linewidth laser diode, whose wavelength was tuned to the wavelength at full-width half-maximum of the FBG spectrum. The PZT was then used to generate Lamb waves in the plate. The strain pulse shifted the FBG sensor spectrum, resulting in a modulation of the measured reflected optical intensity. They were capable of detecting the arrival time of the first symmetric mode Lamb wave (S_0). Tsuda *et al.* have developed a conceptually similar wavelength-intensity conversion scheme that is simple and elegant, using a second FBG sensor (acting as an analyser) and a broadband light source in the place of the laser diode [16]–[18].

In the current work, we present the development of a nervous system using FBG sensors, suitable for integration in our self-healing carbon-fibre composite and capable of localising impact events. We combine an FBG remote sensing system based on Tsuda *et al.'s* work, and a sequentially iterative algorithm developed to localise impacts in orthotropic plates [21]. This algorithm has previously been validated using PZT sensors but, to the authors' knowledge, never with FBG sensors. The algorithm is first tested using PZT sensors as their response to ultrasonic shock pulses is well understood. The PZTs are replaced with FBGs once the system is optimised. Unlike previous studies, where ultrasonic pulses were generated with a PZT emitter and the shape of the signal passed through a damaged region was compared with the signal passed through a healthy region, e. g. [15, 19, 20], the source of the wave in this study is the impact itself, i.e. e. the sensing system is passive.

2. FIBRE BRAGG GRATING (FBG) SENSOR

2-1. Principle of operation

A fibre Bragg grating is a periodic variation of the refractive index of the core of an optical fibre. When illuminated with a broadband light source a narrowband spectrum is reflected—the *Bragg wavelength*, λ_b - whose value satisfies the Bragg condition:

$$\lambda_b = 2n\Lambda \tag{1}$$

where n is the refractive index and Λ is the grating pitch. The FBG can be used as a highly sensitive strain sensor by monitoring the value of the Bragg wavelength, which varies proportionally with the strain state of the FBG. However, this method of strain monitoring requires the use of an optical spectrum analyser, which has a typical sampling rate of a few hertz.

2-2. Ultrasonic damage detection

In the wavelength-intensity conversion technique, the shift in Bragg wavelength of an FBG sensor is converted into an optical light intensity. Figure 1 is a schematic of the principle of operation [16, 17]. A broadband light source is passed through an optical circulator, which allows the narrowband reflected pulse to be routed into an FBG analyser, designed with a peak light transmission of a slightly lower frequency than that of the sensor on the sample. The light transmitted through the analyser is detected by a high-speed photodetector and a fast-sampling digital oscilloscope records the signal. The amount of light reaching the photodetector depends on the overlap between the sensor reflectivity (solid curve) and the analyser transmissivity (dashed curve). When a strain pulse passes the FBG sensor, it causes a small shift of the reflected wavelength under compression (left panel) or tension (right hand panel). This changes the intensity of the light transmitted through the analyser (shaded area) and is recorded as a fast electrical pulse from the photodetector by the digital oscilloscope.

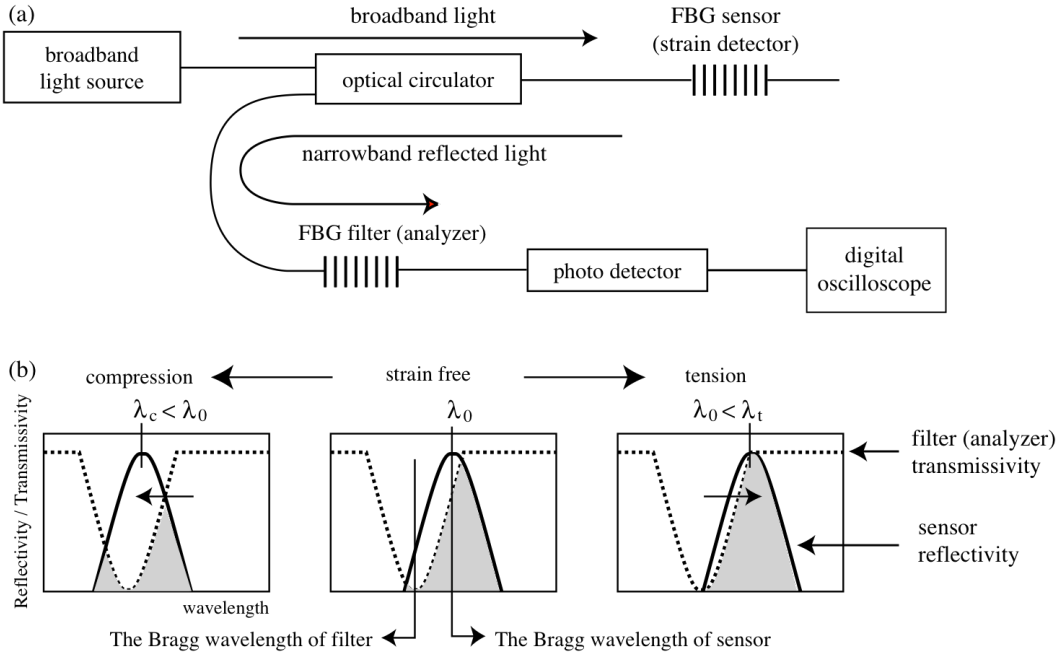

Figure (1) Principle of operation of the FBG fast-sampling readout scheme [16, 17].

3. EXPERIMENTAL

3-1. Materials

A standard carbon-fibre non-crimp fabric (NCF; Saertex) made of Toray T-700 12K yarns was used as the reinforcing fibre bed. Carbon fibres were chosen as they are readily available, are relatively light and stiff, and are used in many structural commercial applications. A [0°/90°] non-crimp fabric was chosen because of its superior drapability and good mechanical properties. The fibres have a tensile strength of 4,900 MPa, a Young's modulus of 230 GPa, a density of 1.8 g cm^{-3} and each UD ply of the fabric has an areal weight of 150 g m^{-2}.

The matrix was a two-part epoxy system consisting of EPON 828 monomer (Shell Chemicals) and diethylenetriamine (DETA) low-temperature hardener (Sigma-Aldrich). The monomer was a diglycidyl ether of bisphenol A, referred to as DGEBA. The EPON 828 was mixed with the DETA in a 100:12 mass ratio. Square composite plates, 500x500x0.85mm^3, with $[0°,90°]_s$ stacking sequence, were prepared by vacuum bag infusion. The standard processing cycle was a 24 hr cure at room-temperature followed by a 24 hr post-cure at 35°C.

The PZT sensors were *Physical Acoustics Corporation (PAC)* nano-30 transducers, connected to a 40 dB 1220 A preamplifier from *PAC*. The FBG sensors were written on SMF28 silica-based optical fibre with diameters of 8 μm, 125 μm and 250 μm for the core, first cladding layer and second cladding layer, respectively. The sensors had Bragg wavelengths of 1542 nm, 1547 nm or 1562 nm, and typically had a gauge length of 4 mm and a reflectivity of 60 %. The strain and temperature dependencies of the FBGs were 1.2 pm/με and 10.6 pm/°C, respectively.

3-2. Composite mechanical properties

Composite samples 25 mm wide, 250 mm long and 0.85 mm thick with $[0°,90°]_s$ stacking sequence were cut with the fibres in the two outer plies parallel to the long axis. Samples were prepared and tested in tension in accordance to the ASTM standards D 3039 and D 3518. Two *HBM* strain gauges, type 10/120LY41 - one to measure longitudinal strain and the other transverse strain - were glued to the surface of each sample, and connected in a half-bridge configuration. The gauges were calibrated before testing. The sample was then clamped in the grips of a tensile tester, and loaded in tension at a rate of 2 mm/min, recording the load-extension data. This test was repeated four times and the values averaged. From this data the tensile moduli (E_{11}, E_{22}) and the Poisson ratios (υ_{12}, $\upsilon_{21}= \upsilon_{12}E_{22}/E_{11}$) were determined. E_{66} was determined by repeating the above procedure on composite samples cut with their plies at $[+45°,-45°]_s$. Finally, E_{12} is given by $\nu_{12}E_{22}/(1-\nu_{12}\nu_{21})$.

3-3. Lamb wave velocity measurement

Two PZTs were mounted on the surface of the plate 100 mm apart, using vacuum grease as a coupling agent. Lamb waves were excited by breaking a 0.5 mm pencil lead on the plate surface behind the first sensor. The signals were detected by the sensors, amplified and recorded by a *Vallen* AMS-Y high-speed AE (acoustic emission) system. The Lamb wave velocity was then determined by dividing the distance between the sensors by the time-of-flight. The velocity of the S_0 mode was determined from the arrival times of the leading edge of the signals. However, the A_0 mode is dispersive at these relatively low frequencies, meaning that the different frequencies have different velocities. Wavelet transform analysis, which breaks down a signal into the time-frequency domain, was therefore used to determine this velocity. From this, the time-of-flight of any given frequency

could be determined. As the composite plate was orthotropic, the measurement was repeated for orientations from 0° to 90° in 15° increments, Fig.2, where the 0° direction was parallel to the carbon fibres in the top lamina.

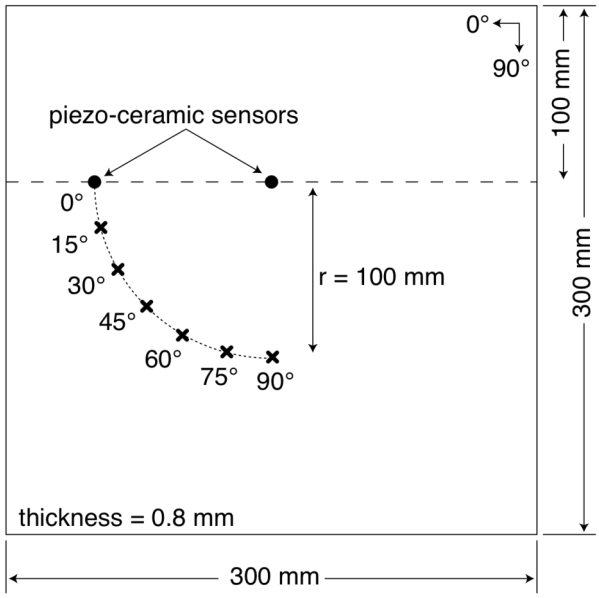

Figure (2) Schematic of the setup to measure the Lamb wave velocity in a $[0°,90°]_s$ carbon fibre composite plate, at different angles to the fibre orientation.

The velocities for the extensional and the flexural modes of orthotropic composites can be predicted from classical plate theory. The assumptions used and full details of the derivation can be found in [22]–[24], for example. The equations relating the extensional velocities to the mechanical properties are

$$c_{e0} = \sqrt{\frac{A_{11}}{\rho h}} \qquad c_{e45} = \sqrt{\frac{(A_{11} + 2A_{66} + A_{22}) + \sqrt{R}}{4\rho h}} \qquad c_{e90} = \sqrt{\frac{A_{22}}{\rho h}} \tag{2}$$

for the 0º, 45º and 90º directions, respectively, where

$$R = (A_{11} + 2A_{66} + A_{22})^2 - 4(A_{11} + A_{66})(A_{22} + A_{66}) + 4(A_{12} + A_{66})^2 \tag{3}$$

and where A_{ij} are the in-plane stiffness values of the laminate, h is the sample width and ρ is its density. A_{ij} is related to the Young modulus by

$$A_{ij} = hQ_{ij} = \frac{E_{ij}}{(1 - \nu_{ij}^{\,2})} \tag{4}$$

where Q_{ij} is the in-plane stiffness values of the lamina, h is the sample width and E_{ij} is the Young modulus. This theory can be extended to include the flexural mode, detailed in [23, 25]. When the laminate contains only 0º and 90º plies,

$$c_{f0} = \sqrt[4]{\frac{D_{11}}{\rho h}}\sqrt{\omega} \qquad c_{f45} = \sqrt[4]{\frac{D_{11} + 2(D_{12} + 2D_{66}) + D_{22}}{4\rho h}}\sqrt{\omega} \qquad c_{f90} = \sqrt[4]{\frac{D_{22}}{\rho h}}\sqrt{\omega} \tag{5}$$

for the 0º, 45º and 90º directions, respectively, where D_{ij} are thebending stiffness values of the material.

3-4. Impact localisation method

The impact is localised using an algorithm based on work by Jeong *et al.* [21]. It is an iterative algorithm, based on an optimisation scheme that minimises an error function. The geometry is shown schematically in Fig. 3, where S_0, S_1 and S_2 are the sensors and P(x,y) is the unknown impact point. The only prior knowledge needed is the position of the three sensors and the velocity versus propagation angle profile. The algorithm considers the difference in arrival time of the signal between the S_0/S_1 sensor pair and defines a locus whose points satisfy this difference. This is repeated for the S_0/S_2 sensor pair, and the intersection of the two loci is the experimental impact point. Full details can be found in [21].

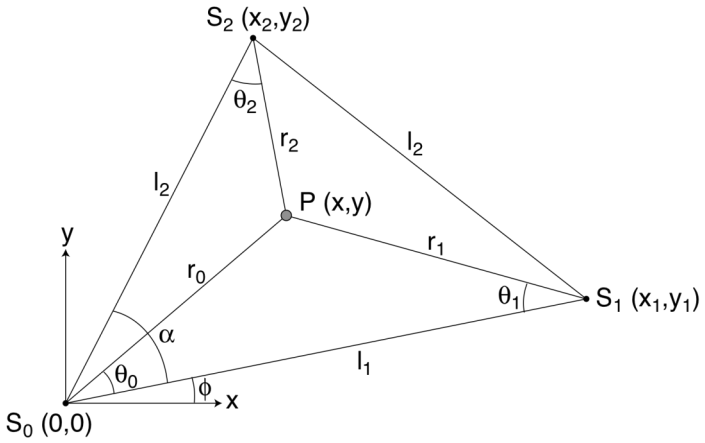

Figure (3) Impact localisation geometry for an anisotropic plate with three sensors (S_i, i= 1,2,3) [21]. The impact occurs at the point P(x,y).

3-5. Localisation with PZT

A 500 x 500mm^2 composite plate was used for the localisation tests with PZTs. The sensors were similar to those used in paragraph 3.3 and were placed at (100,100), (400,100) and (100,400), with the origin in the bottom left corner of the plate. Pencil lead breaks were performed at (150,300), (200,200), (300,140) and (400,350) and the transient signals recorded by the sensors. Localisation of the impact point was based on the arrival times of the S_0 mode.

3-6. Localisation with FBG

A schematic of the hardware setup for localising with three FBG sensors is shown in Fig. 4. The FBG sensor/filter pairs had Bragg wavelengths of 1542 nm, 1547 nm and 1562 nm, and were located at (60,42), (236,17) and (186,143), respectively, on a 300 x 200 mm^2 plate. The sensors were glued on the surface of the plate with Loctite 401 glue. The filters were each mounted on a micrometer stage to precisely control their Bragg wavelength. A broadband 25dBm *Amonics* light source with spectral range 1,528-1,608 nm was used to interrogate the three sensors. The three reflected narrowband signals each passed through their own filter, which had a Bragg wavelength tuned to be slightly offset to that of each sensor. The transmitted light was detected by three *New Focus* 125 MHz low-noise photodetectors, sensitive in the 900-1,700nm range. The outputs from

these photodetectors were read by a high-speed *National Instruments* DAQ at 10 MS/s and recorded in a *LabView* program.

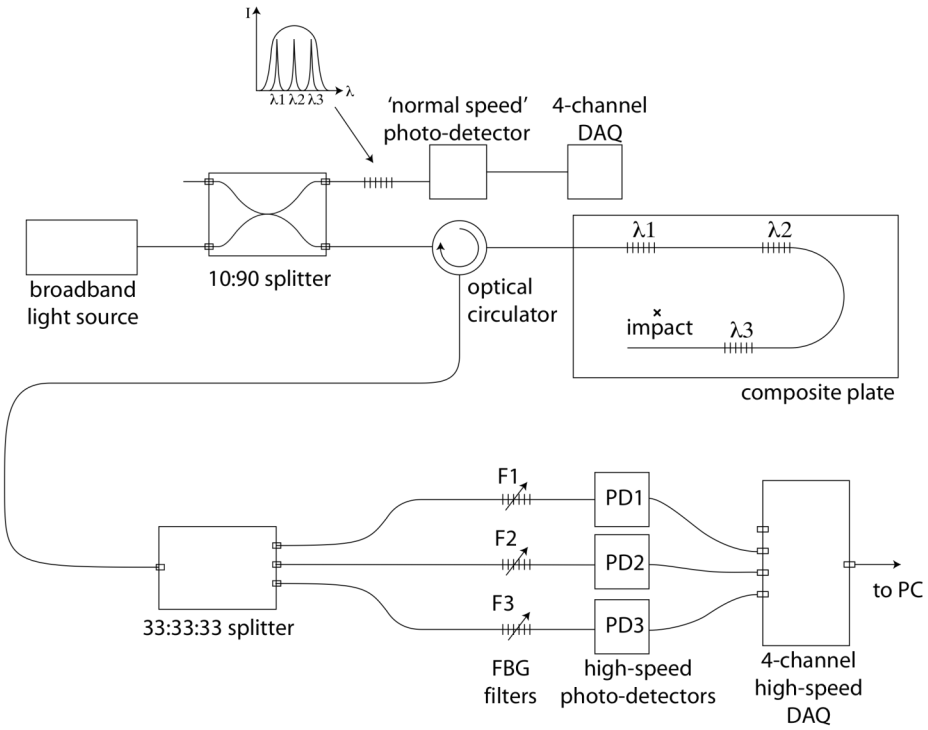

Figure (4) Schematic of the FBG fast-sampling system currently under development. It involves three FBG sensors written on a single fibre, which will allow location of the impact point.

4. RESULTS AND DISCUSSION

4-1. Composite mechanical properties

The tensile samples were tested as described in paragraph 3.2, to determine the mechanical properties. Example stress-strain curves are shown in Figs. 5 and 6, and the measured and calculated properties are summarised in Table 1. Five samples were tested in each case.

Table (1) Experimentally-determined values of the mechanical properties of the composite laminate with [0,90]s layup. E_{ij} is the tensile stiffness, D_{ij} the flexural stiffness, ν_{ij} the Poisson ratio and ρ the density.

E_{11}, E_{22} [GPa]	E_{66} [GPa]	E_{12} [GPa]	ν_{12},ν_{21}	D_{11}, D_{22} [Pa m^3]	D_{66} [Pa m^3]	D_{12} [Pa m^3]	ρ [kg m^{-3}]
47.7±0.3	5.55±0.4	1.32	0.028	2.44	0.28	0.068	1214

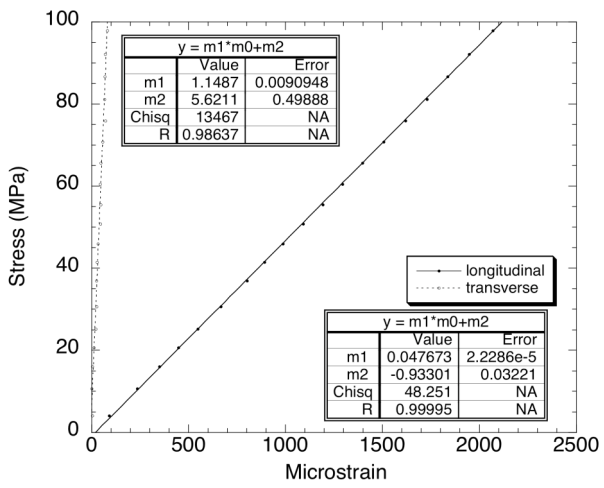

Figure (5) Longitudinal and transverse stress strain curves in the 0º direction of the composite. The transverse strain is negative in reality but shown here as positive for clarity.

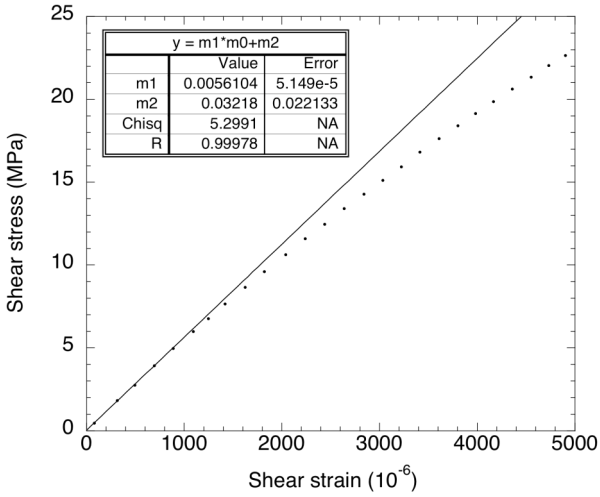

Figure (6) Stress strain curve for composite samples cut with their carbon fibres at ±45º to the long axis.

4-2. Lamb wave velocity measurement

The theoretical velocities were calculated using Eqs. 2-6 and the values in Table 1. The experimental velocities of the S_0 and A_0 modes were then determined with two PZT sensors as described in paragraph 3.3. Figure 7 shows typical signals recorded by the two sensors, placed 100mm apart, and Figs. 8 and 9 are the resulting S_0 and A_0 velocity profiles, respectively. Table 2 gives the theoretical and experimental velocities of the S_0 mode and of the 30 kHz A_0 mode. The theoretical and experimental values for the S_0 mode are in good agreement. The experimental values for the A_0 mode, however, were substantially higher than predicted. Further work is needed to explain this discrepancy.

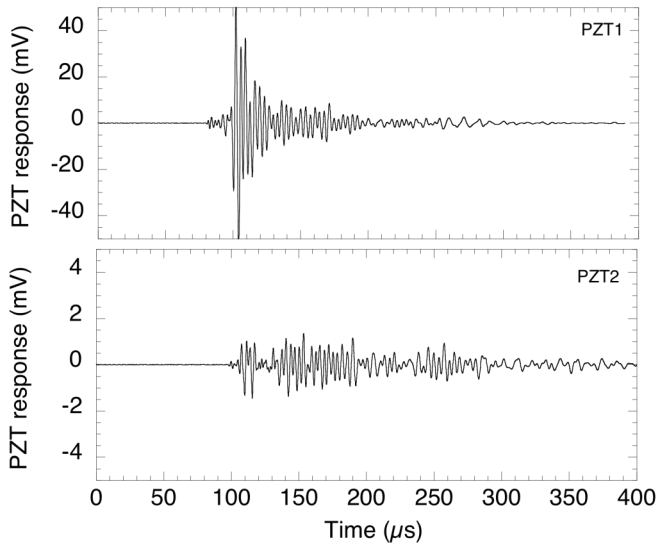

Figure (7) Signals from two PZT sensors mounted 100mm apart on the surface of the plate, at 75º to the fibre direction. Note the different y-axis scales for the two plots.

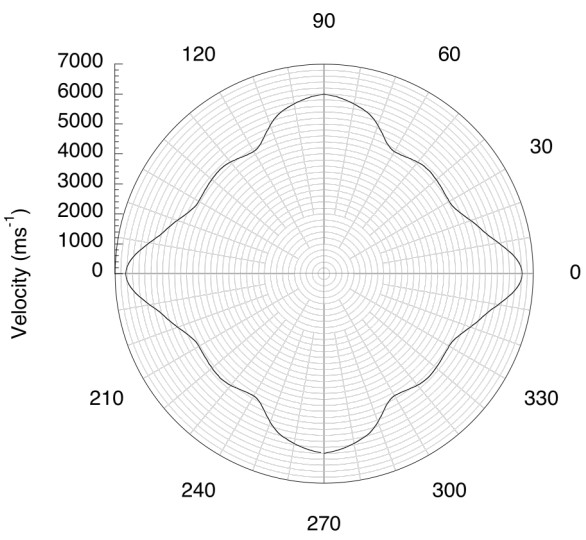

Figure (8) Velocity of the S_0 mode for the 500x500mm^2 composite panel. Zero degree is parallel to the carbon fibre long axis in the top ply.

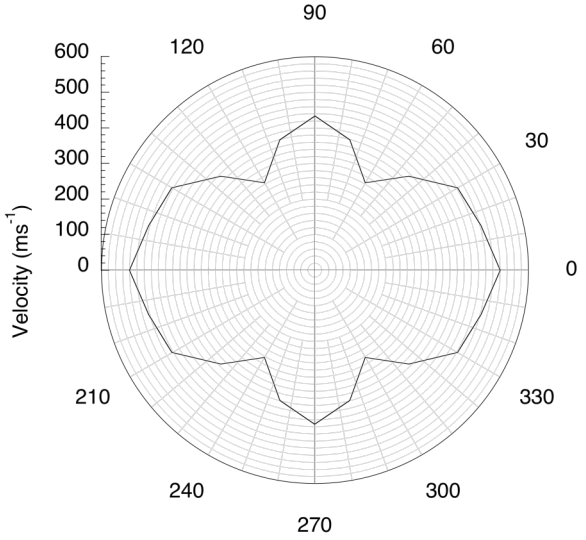

Figure (9) Velocity of the A_0 mode at 30kHz for the 300x200mm^2 composite panel. Zero degree is parallel to the carbon fibre long axis in the top ply.

Table (2) Comparison of theoretical and experimental Lamb wave velocities in the $[0,90]_s$ composite plate.

	S_0		A_0 (30kHz)	
Angle [°]	Theoretical [ms^{-1}]	Experimental [ms^{-1}]	Theoretical [ms^{-1}]	Experimental [ms^{-1}]
0, 90	6,270	6,630	215	520
45	4,970	4,920	191	433

4-3. Impact localisation with PZT sensors

Pencil lead breaks were made at (150,300), (200,200), (300,140) and (400,350), and recorded with the Vallen system. Figure 10 is an example of a lead break at (300,140). The three solid dots are the positions of the three PZT sensors. The dashed vertical line and the solid horizontal line are the loci of possible solutions whose coordinates satisfy the time-of-flight difference between the (100,100)/(400,100) sensor pair and the (100,100)/(100,400) sensor pair, respectively. The crossing point is the localisation solution, and is (297.4, 143.8) in this case. All trials are summarised in Fig. 11, with average errors of 10.5 mm in x and mm in 6.0 y.

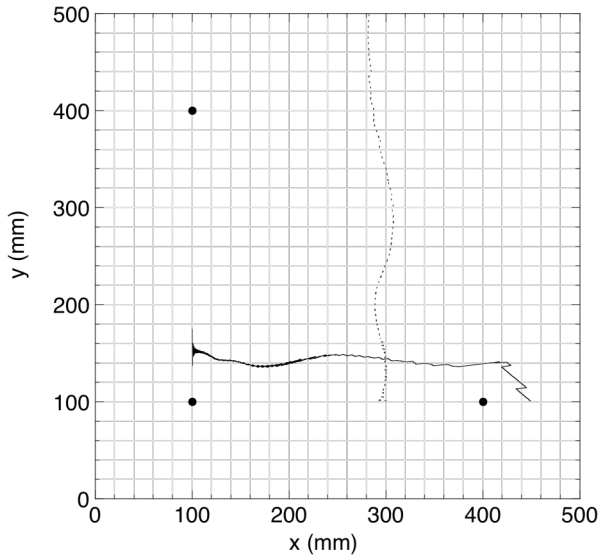

Figure (10) Experimental localisation of an impact at (300,140) in a composite plate using the Jeong et al. algorithm. The three dots show the PZT sensor locations.

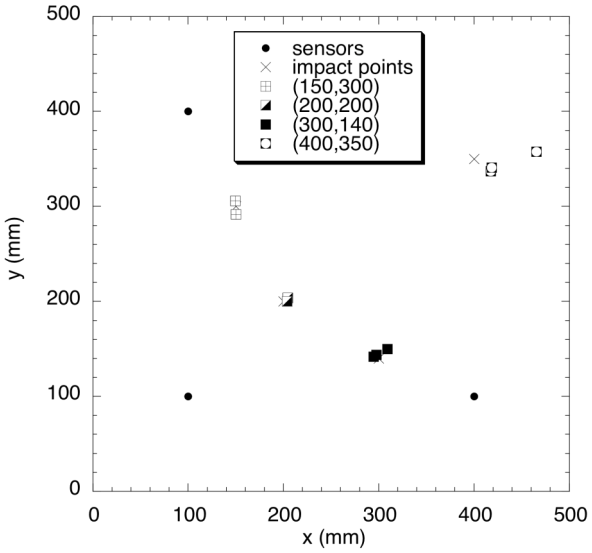

Figure (11) Pencil lead break localisation in the composite plate with three PZT sensors, and using the Jeong at al. algorithm.

4-3. Impact localisation with FBG sensors

First measurements of impact localisation with FBG sensors have begun. Figure 12 shows a typical FBG intensity signal measured by one of the photodetectors. The time scale here is significantly longer than in the case of the PZT signal, Fig. 7. In addition, there is more background noise in the case of the FBGs. However, the arrival time of the pulse remains clearly visible.

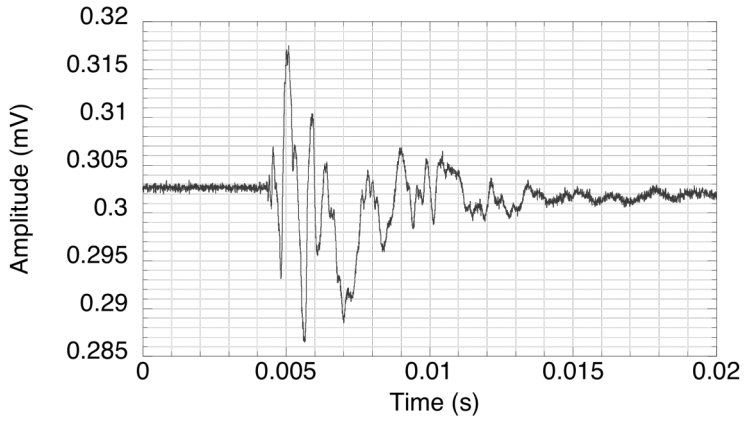

Figure (12) Typical response of a surface-mounted FBG sensor to a pencil lead break.

The localisation results with FBG sensors for pencil lead breaks at (150,100) are shown in Fig. 13. These are promising first results, showing good repeatability, with an average error of 7.2 mm in x and 3.5 mm in y. However, these results represent work-in-progress, and focus is currently on FBG signal processing and optimisation of the localisation using the A_0 mode.

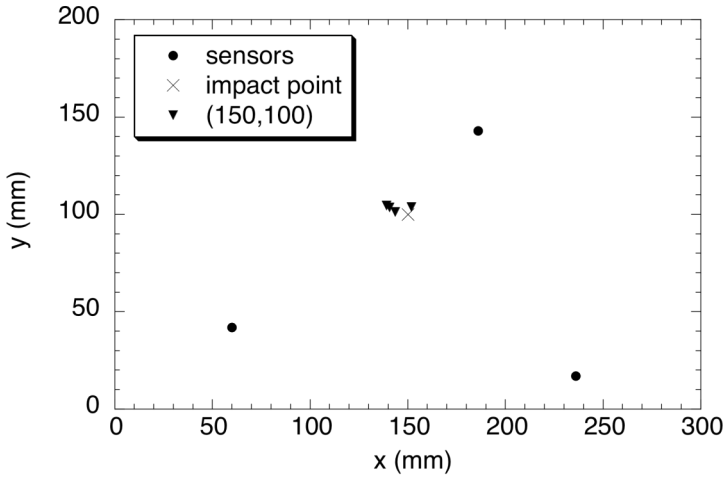

Figure (13) Pencil lead break localisation in the composite plate with three FBG sensors, and using the Jeong *et al*. algorithm.

5. CONCLUSION

We have shown that it is possible to locate an impact on a composite plate using three surface-mounted fibre Bragg grating sensors to monitor ultrasonic Lamb waves, to a precision of a few millimetres. To do so we combined a novel wavelength-intensity conversion technique that allows fast-sampling of the FBGs, and a sequentially-iterative algorithm for localising an impact on an orthotropic plate. To our knowledge, this is the first time this combination has been developed.

The algorithm was first verified by using three surface-mounted piezo-ceramic transducers, as their response to ultrasonic pulses is well understood. The PZT sensors were then replaced with FBG sensors, once the algorithm was optimised. While the PZTs showed a higher sensitivity to the shock pulse, the FBGs were capable of detecting lower frequencies of the pulse. Localisation with the PZT sensors can be based on the first symmetric (S_0) mode. However, localisation with FBG sensors needs to be based on the A_0 mode, as the S_0 mode is relatively small in amplitude and is lost in the noise of the FBG acquisition system. Localisation with the A_0 mode is more complex than with the S_0 mode, as the A_0 mode velocity varies sharply with frequency. The next steps will be in optimising both the post-processing of the FBG signal, and the localisation based on a specific frequency of the A_0 mode.

ACKNOWLEDGEMENTS

The authors gratefully acknowledge the financial support of the Swiss National Science Foundation (contract no.200020-105169). R. de Oliveira is a fellow of the Portuguese Foundation for Science and Technology (FCT contract number SFRH/BPD//41347/2007).

REFERENCES

1. S.R. White, N.R. Sottos, P.H. Guebelle, J.S. Moore, M.R. Kessler, S.R. Sriram, E.N. Brown and S. Viswanathan, "Autonomic healing of polymer composites," Nature, 409, 794-797 (2001).
2. E.L. Kirkby, J.D. Rule, V.J. Michaud, N.R. Sottos, S.R. White and J.-A.E. Månson, "Embedded shape memory alloy wires to improve performance of self-healing polymers," Advanced Functional Materials, 18, 22532260 (2008).

3. H. Lamb, "On waves in an elastic plate," Proceedings of the Royal Society of London, 93, 114-128 (1917).
4. A.H. Nayfeh, M.J. Anderson, "Wave propagation in layered aniostropic media with applications to composites," The Journal of the Acoustical Society of America, 108, 471-472 (2000).
5. J. Rose, "Ultrasonic waves in solid media," Cambridge: Cambridge University Press, 10131 (1999).
6. G. Zhou, L.M. Sim, P.A. Brewster and A.R. Giles, "Through-the-thickness mechanical properties of smart quasi-isotropic carbon/epoxy laminate," Composites A, 35, 797-815 (2004).
7. Y. Okabe, T. Mizutani and S. Yashiro, "Detection of microscopic damages in composite laminates with embedded small-diameter fiber Bragg grating sensors," Composites Science and Technology, 62, 951-958 (2002).
8. W.W. Morey, G. Meltz, W.H. Glenn, "Fiber Bragg grating sensors," Proceedings of SPIE, 1169, Fiber Optic and Laser Sensors VII, 98-107 (1989).
9. W.W. Morey, J.R. Dunphy, G. Meltz, "Multiplexing fiber Bragg grating sensors." Proceedings of SPIE, 1586, Distributed and Multiplexed Fiber Optic Sensors, 216-224 (1991).
10. Y. Okabe, S. Yashiro, T. Kosaka, N. Takeda, "Detection of transverse cracks in CFRP composites using embedded fiber Bragg grating sensors." Smart Materials and Structures, 9, 832-838 (2000).
11. Y. Okabe, R. Tsuji, N. Takeda, "Application of chirped fiber Bragg grating sensors for identification of crack locations in composites," Composites A, 35, 59-65 (2004).
12. S. Takeda, S. Minakuchi, Y. Okabe, N. Takeda, "Delamination monitoring of laminated composites subjected to low-velocity impact using small-diameter FBG sensors," Composites A, 36, 903-908 (2005).
13. D.C. Betz, G. Thursby, B. Culshaw, W.J. Staszewski, "Acoutso-ultrasonic sensing using fiber Bragg gratings," Smart Materials and Structures, 12, 122-128 (2003).
14. D.C. Betz, G. Thursby, B. Culshaw, W.J. Staszewski, "Identification of structural damage using multifunctional Bragg grating sensors: I. Theory and implementation," Smart Materials and Structures, 15, 1305-1312 (2006).
15. D.C. Betz, G. Thursby, B. Culshaw, W.J. Staszewski, "Structural damage identification using multifunctional Bragg grating sensors: II. Damage detection results and analysis," Smart Materials and Structures, 15, 1313-1322 (2006).
16. H. Tsuda, N. Toyama, K. Urabe, J. Takatsubo, "Impact damage detection in CFRP using fiber Bragg gratings," Smart Materials and Structures, 13, 719-724 (2004).
17. H. Tsuda, "Ultrasound and damage detection in CFRP using fiber Bragg grating sensors," Composites Science and Technology, 66, 676-683 (2006).
18. H. Tsuda, J.-R. Lee, "Strain and damage monitoring of CFRP in impact loading using a fiber Bragg grating sensor system," Composites Science and Technology, 67, 1353-1361 (2007).
19. S.S. Kessler, S.M. Spearing, C. Soutis, "Damage detection in composite materials using Lamb wave methods," Smart Materials and Structures, 11, 269-278 (2002).
20. J.-R. Lee, H. Tsuda, N. Toyama, "Impact wave and damage detections using a strain- free fiber Bragg grating ultrasonic receiver," NDT&E International, 40, 85-93 (2007).
21. H. Jeong, Y.S. Jang, "Wavelet analysis of plate wave propagation in composite laminates," Composite Structures, 49, 443-450 (2000).
22. W.H. Prosser, "The propagation characteristics of the plate modes of acoustic emission waves in thin aluminium plates and thin graphite/epoxy composite plates and tubes," Ph.D. Dissertation, The Johns Hopkins University, Baltimore, Maryland (1991).
23. J.W. Whitney, "Structural analysis of laminated anisotropic plates," Technomic Publishing Co., Lancaster, Pennsylvania (1987).
24. J.-M. Bertholet, "Materiaux composites, comportement mecanique et analyse des structures," Masson (1992).
25. K.F. Graff, "Wave motion in elastic solids," Universities Press, Belfast (1975).